ADAPTIVE MISMATCHED FILTER DESIGN
FOR RADAR PULSE COMPRESSION

VIKAS BAGHEL

Jaypee University of Information Technology,
Waknaghat Solan, Himachal Pradesh, 173234, India
Email: vikas.baghel@juit.ac.in

Abstract

Adaptive Pulse Compression (APC) techniques for target detection differ from their mismatched filtering techniques based counterparts in their improved ability to detect the target efficiently. In order to further improve the target detection capability, an attempt has been made to design a novel pulse compression model, named Adaptive Mismatched Filter (AMMF). The AMMF consists of a linear network of fixed weights followed by an adaptive linear network. An adaptive algorithm based on Minimum Mean-Square Error (MMSE) has been suggested to estimate the weight coefficients of the adaptive network. The performance analysis of the new adaptive model has been carried out using an extensive simulation study. The detection efficiency of the proposed scheme, in terms of Peak Signal-to-sidelobe Ratio (PSR), Integrated Sidelobe Ratio (ISLR) and Average Target Power Prediction Accuracy (ATPPA), has been compared with that obtained using other existing APC techniques. The simulation study reveals the enhanced detection ability of the proposed AMMF.

Keywords: Adaptive pulse compression, Matched filter, Minimum mean square error, Mismatched filter, Pulse compression.

1. Introduction

The conventional Matched Filter (MF) is commonly employed for radar pulse compression [1]. The output response of matched filtering contains the large sidelobes in the multiple moving targets environment. Sometimes these large sidelobes form spurious targets or sometimes mask weak neighbouring targets. In addition, sidelobe suppression using mismatched filtering techniques have been of considerable interest to the research community over many years. Ackroyd and Ghani [2] explained that an inverse filtering technique based on least-mean-square approximation has been employed for mismatched filter design. For different barker sequences, the authors have reported complete suppressed sidelobes with a small loss in SNR compared to the MF. Zoraster [3] has proposed a linear programming technique based approach for mismatched filter design and manage to achieve 5dB lower peak sidelobes as compared to the least square filter.

Baden and Cohen [4] have proposed by using a weighted sidelobe reduction filtering technique, a mismatched filter model of low complexity. In this paper, weightage functions have been used to shape the sidelobe energy for the orthogonal code pairs. Fuentes and Fam [5] reported that the mismatched filter used sidelobe inversion method [5]. To reduce the chip area and power requirement for VLSI implementation, a cascade structure of matched filter and multistage-filter has been used in this paper. Levanon and Scharf [6] proposed in comparing the parallel outputs of contrasting mismatched filters, a range sidelobe blanking technique. Kumari et al. [7] suggested using a modified Woo filter to achieve low sidelobe pattern for P4 polyphase code. In this model, two time-shifted received pulses are combined and then correlated with the transmitted pulse to get the desired output. Akbaripour and Bastani [8] suggested using the two multi-stage mismatched filters based on linear programming technique and Lagrange multiplier method. In this paper, an iterative approach has been proposed to yield desired PSR by shaping the sidelobe energy with the help of weighting functions.

Blunt and Gerlach [9] worked on one of the pioneering articles in the field of pulse compression, where authors presented the MMSE based adaptive pulse compression algorithm for the efficient sidelobe reduction and illustrated its ability to detect large and small targets in noisy condition. Blunt et al [10, 11] proposed for multiple non-stationary target detection, another variant of modified APC algorithm, named Doppler-compensated APC algorithm (DC-APC). Interestingly, in the work, the DC-APC algorithm suppresses the range sidelobes resulting from moving targets and estimates the true range profile.

Due to the use of adaptive pulse compression filter for each individual range cell of interest, the computational cost of this adaptive approach is very high. Based on decimated and contiguous signal models a FAST adaptive pulse compression algorithm (FAPC) has been proposed to reduce the computational complexity of the APC [12]. Baghel and Panda [13] proposed the multiple stationery and non-stationary target conditions, which is a generalized adaptive pulse compression (G-APC) algorithm and has been shown to provide better results in comparison with APC and DC-APC algorithms. In this paper, the change in the phase of the received signal due to the Doppler shift is incorporated into the signal model. Wang et al. [14] used the practical application of solid-state radars, which is the APC algorithm for weather observation, near-surface precipitation measurement and for air traffic observation. Based on studies by Kikuchi et al. [15], an MMSE based pulse

compression method has also been used in the application of X-Band phased array weather radar.

A similar MMSE based scheme presented recently by Li et al. has the advantage of low computational complexity. In this paper, authors have shown that the complexity of the proposed filtering method is similar to that of matched filtering [16]. According to Dominguez et al. [17], the APC technique was applied to range compression in SAR image focusing and evaluated under real and ideal conditions. In contrast to traditional methods, APC was shown to preserve resolution and reduce sidelobes with only marginal SNR loss. Cuprak and Wage [18] presented the application of covariance matrix tapers (CMTs) to the RMMSE algorithm for robust performance against Doppler. The computational efficient RMMSE-CMT model was shown to be robust in a variety of simulations and performs well even past the designed Doppler shift. Shokooh and Okhovvat [19] proposed a new method to account for both the Doppler phase shift and pulse eclipsing by using the Modified Adaptive Pulse Compression Repair (MAPCR) algorithm. The proposed MAPCR algorithm based on adaptive post-processing, not only innovates in repairing the eclipsed regions, but also applies the MF-RMMSE algorithm for the centre of processing window (non-eclipsed region).

To utilize the advantages of APC algorithm, which locally construct an adaptive filter for each individual range cell, an attempt has been made in this paper to design a new pulse compression model, which incorporates the concept of APC along with matched filtering. In this proposed model, a fixed-weighted linear network is followed by an adaptive linear network. The weight coefficients of the adaptive network are identified using the MMSE based adaptive algorithm. Enhanced performance is expected at a lower computational cost in comparison with previously proposed adaptive pulse compression techniques. The paper is organized as follows. The proposed pulse compression model (AMMF) is presented in Section 2. Sequentially, an MMSE based adaptive algorithm for the proposed AMMF model is outlined in Section 3. Extensive simulations have been carried out in Section 4 to demonstrate the efficacy of the proposed AMMF in different target scenarios. Lastly, the conclusions of the paper are presented in Section 5.

2. Proposed Adaptive Mismatched Filter (AMMF) Model

The proposed AMMF model for pulse compression is shown in Fig. 1, in which, D denotes a time delay. This AMMF model is composed of a fixed-weighted linear network and an adaptive linear network. Each output of the first linear network is the weighted sum of the adjacent delayed inputs. The weight coefficients of this network are fixed and equal to the complex conjugate of the transmitted waveform, similar to the MF's weight coefficients. The output of the first linear network can be expressed as:

$$z(l) = B^H r(l) \tag{1}$$

where the vector $z(l) = \left[z_0(l), z_1(l), \ldots, z_{(N/2)-1}(l) \right]^T$ represents the output of the first stage and $r(l) = [r(l), r(l+1), \ldots, r(l+N-1)]^T$ represents a vector of N contiguous discrete samples of the received signal. Here $r(l)$ is the lth delayed received sample of the processing window of length, L. Note that $(.)^H$ and $(.)^T$

represent the Hermitian and transpose operations, respectively. The B represents the weight coefficients matrix $\left(N \times \frac{N}{2}\right)$ of the first linear network and is given as:

$$B = \begin{bmatrix} s_0 & 0 & 0 & 0 & & \cdots & 0 \\ s_1 & 0 & 0 & 0 & & \cdots & 0 \\ 0 & s_2 & 0 & 0 & & \cdots & 0 \\ 0 & s_3 & 0 & 0 & \cdots & & 0 \\ \vdots & \vdots & \vdots & \vdots & & \ddots & \vdots \\ 0 & 0 & 0 & 0 & \cdots & & s_{N-2} \\ 0 & 0 & 0 & 0 & \cdots & & s_{N-1} \end{bmatrix} \tag{2}$$

where $s = [s_0, s_1, \ldots, s_{N-1}]^T$ represents N samples of the transmitted pulse. The final output of the proposed model $x_{out}(l)$ can be written as

$$x_{out}(l) = w^H(l)z(l) \tag{3}$$

where $w(l) = \left[w_0(l), w_1(l), \ldots, w_{(N/2)-1}(l)\right]^T$ represents the weight coefficients of the adaptive stage. From Eq. (1), the simplified model output is

$$x_{out}(l) = w^H(l)B^H r(l) \tag{4}$$
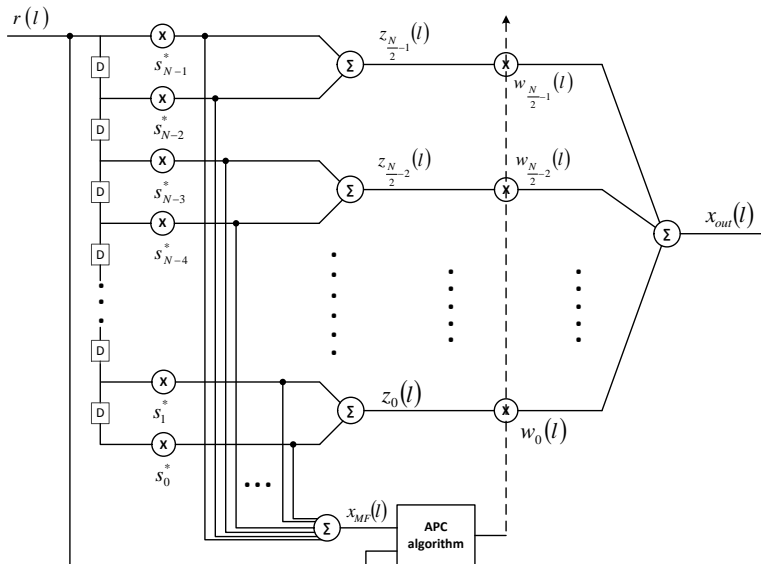

Fig. 1. Adaptive mismatched filter (AMMF) model.

3. Adaptive Pulse Compression algorithm for AMMF

The Doppler shifted discrete received signal model [13] can be written as

$$r(l) = x^T(l)\big(s + \Delta s(l)\big) + v(l) \tag{5}$$

where $x(l) = [x(l), x(l-1), \ldots, x(l-N+1)]^T$ represents N contiguous impulse response samples of range profile and expression $v(l)$ is the additive noise. The Doppler phase shift is induced by the moving target, which results the phase shift in the reflected signal with respect to the transmitted signal. Therefore, the reflected signal can be modelled as given in Eq. (5), where $\Delta s(l) =$

$[\Delta s_0(l), \Delta s_1(l), \ldots, \Delta s_{N-1}(l)]^T$ represents N contiguous sample-by-sample change in the transmitted signal contributed by the Doppler shift. The N contiguous samples of received signal, collected at the receiver end, can be written as

$$r(l) = X^T(l)\big(s + \Delta s(l)\big) + v(l) \tag{6}$$

where $v(l) = [v(l), v(l-1), \ldots, v(l+N-1)]^T$. Here $X(l)$ represents the N length-N sample-shifted snapshots of the impulse response and is given as

$$X(l) = \begin{bmatrix} x(l) & x(l+1) & \cdots & x(l+N-1) \\ x(l-1) & x(l) & \ddots & \vdots \\ \vdots & \ddots & \ddots & x(l+1) \\ x(l-N+1) & \cdots & x(l-1) & x(l) \end{bmatrix} \tag{7}$$

To estimate the range profile impulse response of each range cell with the help of the proposed model, the standard MMSE cost function can be designed as

$$J(l) = E[|x(l) - x_{out}(l)|^2] \tag{8}$$

Here, $E[\ ]$ denotes statistical expectation. From Eq. (4), above equation can be formulated as

$$J(l) = E[|x(l) - w^H(l)B^H r(l)|^2] \tag{9}$$

To minimize the MMSE for each individual delay index, the above cost function is differentiated with respect to $w(l)$ and $\Delta s(l)$.

$$\underset{w(l),\Delta s(l)}{\underline{Minimize}}\ E\left[\left|x(l) - w^H(l)B^H\big\{X^T(l)\big(s + \Delta s(l)\big) + v(l)\big\}\right|^2\right] \tag{10}$$

To minimize this cost function, first, we find the optimum value of $\Delta s(l)$, $\Delta s_{op}(l)$, and then by using this optimum value, we find the weight coefficients of the adaptive stage. To find $\Delta s_{op}(l)$, we need to make assumption about $w(l)$. To reduce processing time and computational complexity, we have assumed that the weight coefficients for l^{th} range cell are equal to the output of the first linear network, that is $w(l) = z(l)$. Using this assumption, Eq. (10) can be rewritten as

$$\underset{\Delta s(l)}{\underline{Minimize}}\ E\left[\left|x(l) - z^H(l)B^H\big\{X^T(l)\big(s + \Delta s(l)\big) + v(l)\big\}\right|^2\right] \tag{11}$$

The above minimization function Eq. (11) is quite similar to the function described in Ref. (Eq. (9), [13]). To obtain the optimum value of $\Delta s_{op}(l)$ for each individual range cell, Eq. (11) is differentiated with respect to $\Delta s(l)$ and then the result is set equal to zero. Using assumption $E[z(l)x(l \pm n)] = 0$ for $n \neq 0$, the $\Delta s_{op}(l)$ can be obtained as:

$$\Delta s_{op}(l) = (BG(l)B^H)^{-1}Bz(l) - s \tag{12}$$

where $G(l)$ is

$$G(l) = \begin{bmatrix} z_0(l)z_0^*(l) & & 0 \\ & \ddots & \\ 0 & & z_{(N/2)-1}(l)z_{(N/2)-1}^*(l) \end{bmatrix} \tag{13}$$

By using Eq. (1), we can further simplify the above equation and it becomes

$$\Delta s_{op}(l) = \hat{G}(l)^{-1}r(l) - s \tag{14}$$

where

$$\hat{G}(l) = \begin{bmatrix} r(l)r^*(l) & & 0 \\ & \ddots & \\ 0 & & r(l+N-1)r^*(l+N-1) \end{bmatrix} \tag{15}$$

Equation (14) shows that $\Delta s_{op}(l)$ does not depend on the output of the first network. It can be directly calculated using the received signal. With the help of calculated $\Delta s_{op}(l)$ from Eq. (14), Eq. (10) can be rewritten as

$$\underset{w(l)}{\underline{Minimize}} \ E\left[\left|x(l) - w^H(l)B^H\left\{X^T(l)\left(s + \Delta s_{op}(l)\right) + v(l)\right\}\right|^2\right] \tag{16}$$

Baghel and Panda [13] explained that this minimization equation is similar to the equation. By simplifying Eq. (16), the optimum value of weight coefficients of the adaptive network can be obtained as:

$$w_{opt}(l) = \rho(l)[B^H(C(l) + P(l) + Q(l) + U(l) + R)B]^{-1}B^H\left(s + \Delta s_{op}(l)\right) \tag{17}$$

Here it is assumed that $E[x(l \pm n)x(n \pm m)] = 0$ for $n \neq m$ and $E[x(l)v(l)] = 0$. As described in [9], $\rho(l) = |x(l)|^2$ and R represents noise covariance matrix. Other parameters $C(l), P(l), Q(l)$ and $U(l)$ are obtained as in Eqs. (18) to (21), respectively.

$$C(l) = \sum_{n=-N+1}^{N-1} \rho(l+n)\, \tilde{s}_n\, \tilde{s}_n^H \tag{18}$$

where $\tilde{s}_n$ is the delayed waveform of s shifted by n samples, e.g., $\tilde{s}_2 = [0\ 0\ s_0\ \dots s_{N-3}]^T$ and $\tilde{s}_{-2} = [s_2\ \dots s_{N-1}\ 0\ 0]^T$.

$$P(l) = \begin{bmatrix} \sum_{n=0}^{N-1}\rho(l-n)\Delta s_n(l)s_n^* & & 0 \\ & \ddots & \\ 0 & & \sum_{n=0}^{N-1}\rho(l-n+n-1)\Delta s_n(l)s_n^* \end{bmatrix} \tag{19}$$

$$Q(l) = \begin{bmatrix} \sum_{n=0}^{N-1}\rho(l-n)s_n\Delta s_n^*(l) & & 0 \\ & \ddots & \\ 0 & & \sum_{n=0}^{N-1}\rho(l-n+n-1)s_n\Delta s_n^*(l) \end{bmatrix} \tag{20}$$

$$U(l) = \sum_{n=-N+1}^{N-1} \rho(l+n)\, \Delta\tilde{s}_n(l)\, \Delta\tilde{s}_n^H(l) \tag{21}$$

where $\Delta\tilde{s}_n(l)$ is represented similarly as $\tilde{s}_n$ described in Eq. (18). It represents the delayed samples of $\Delta s_{op}(l)$. We cannot calculate $\rho(l)$ without the prior knowledge of range cell impulse response $x(l)$. Here the matched filtered output is used for evaluating this parameter, $\rho(l) = |x_{MF}(l)|^2$. Blunt, and Gerlach [9], Blunt et al. [11] and Baghel and Panda [13] compared by using direct matched filter output, in which, the computational complexity is further reduced and normalized matched filter output is used for calculating the same.

4. Results and Discussion

For the performance comparison of five different pulse compression methods, NMF [1], APC [9], DC-APC [11], G-APC [13] and proposed AMMF, the Lewis-Kretschmer P3 code [20] of length $N\ (= 30)$ and $L\ (= 100)$ number of range cells
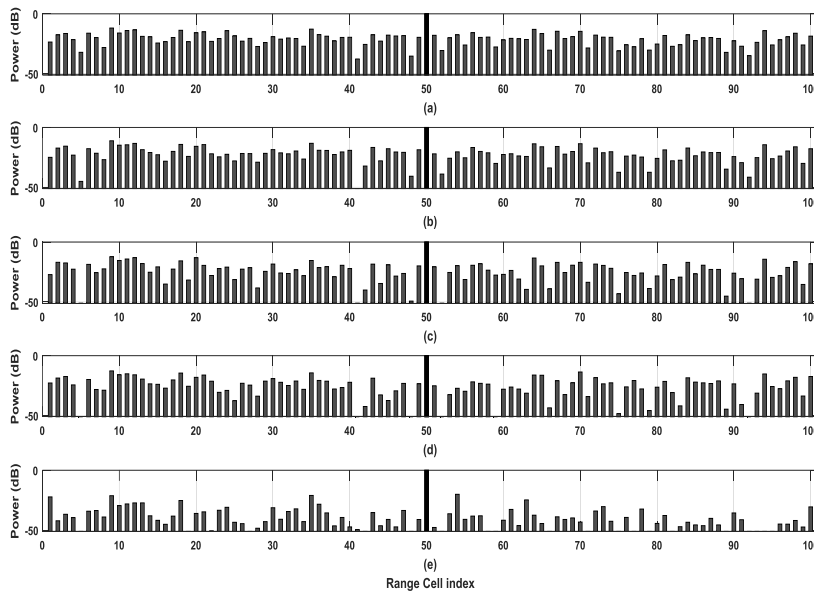
of range profile are used. For all five methods, the performance parameter PSR is obtained through the simulation and compared. The performance comparison in terms of ISLR and ATPPA are also made for several different size targets with severe Doppler shift conditions. Based on stationary and non-stationary targets conditions, five different cases have been studied in this section. The noise is considered to be a uniform white noise with zero mean.

4.1. Case 1: Low SNR stationary point target

In the first case, a low SNR stationary point target is taken into consideration. To simulate this condition, the noise power is taken as $10 dB$ less with respect to the target return. The PSR and ISLR shown in Table 1 indicate the effectiveness of the AMMF over the other methods in highly noisy condition. Figure 2 shows the performance of the proposed AMMF compared to the other pulse compression methods. It is found that the AMMF shows slightly lower side lobes compared to others.

**Table 1. Comparison of PSR_{dB} (and $ISLR_{dB}$) for different SNR conditions.**

	NMF	APC	DC-APC	G-APC	AMMF
Case-1	11.87	11.12	12.26	12.70	20.05
	(1.05)	(0.52)	(-0.48)	(-1.29)	(-12.33)
Case-2	20.24	31.54	29.30	35.66	40.57
	(-10.58)	(-19.68)	(-19.28)	(-24.68)	(-37.01)
Case-3	18.47	20.56	22.42	35.26	36.52
	(-10.16)	(-17.04)	(-17.15)	(-24.19)	(-33.05)

Fig. 2. Estimated range profile impulse response for each individual range cell using (a) NMF, (b) APC, (c) DC-APC, (d) G-APC, (e) AMMF for case-1.

4.2. Case 2: High SNR stationary point target

To simulate this condition, a high SNR point target of $40dB$ above the noise floor is taken. The PSR and ISLR calculated from the outputs of the all five methods are presented in Table 1. These measurements show the proposed AMMF provides better result in comparison to others. It is also confirmed from the outputs of the all five pulse compression methods shown in Fig. 3. The energy of side lobes of the output of AMMF is much lesser than the other techniques. Figure 3 illustrates the results in which, as expected, NMF suffers from range sidelobes. The other methods, however, are able to estimate the range profile down to the level of the noise.
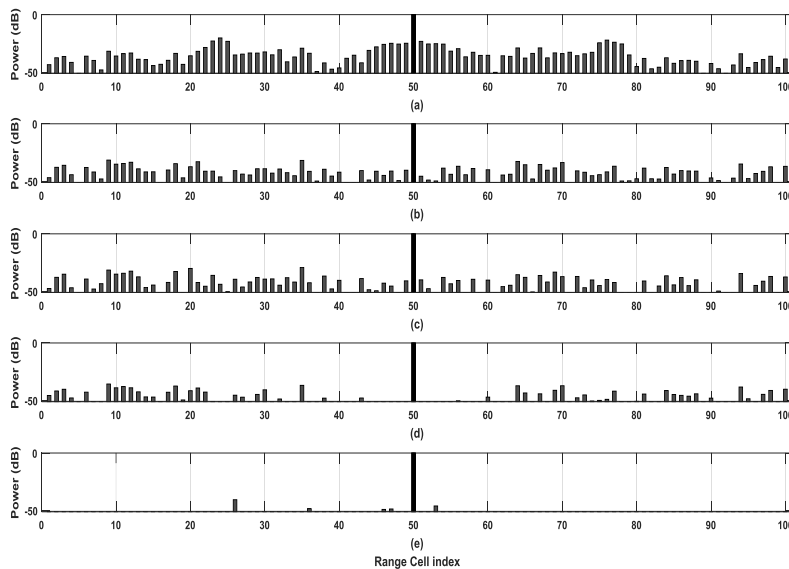
Fig. 3. Estimated range profile impulse response for each individual range cell using (a) NMF, (b) APC, (c) DC-APC, (d) G-APC, (e) AMMF for case-2.

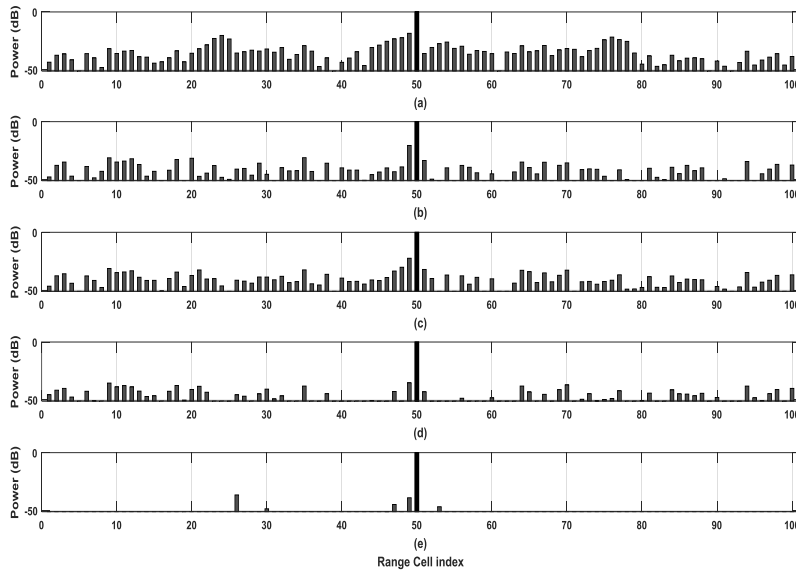## 4.3. Case 3: High SNR non-stationary point target

In this case, a non-stationary point target with high SNR is considered. Because of the moving target, phase shifted return pulses are received at the receiver. To simulate this condition, the received pulse is phase shifted by 20° over the full length of the waveform.

The noise power is taken as 40dB less with respect to the moving target. The PSR and ISLR performance of all five methods for this case have been measured through simulation and are presented in Table 2. The proposed algorithm, while degraded somewhat as a result of Doppler mismatch, is still able to significantly outperform.

The comparative simulation results justify the better performance of the AMMF model under Doppler shift condition. Figure 4 summarises the results for NMF, APC, DC-APC, G-APC and the proposed AMMF. From this, it can be confirmed that the AMMF suppresses sidelobes efficiently when compared to others methods.

Table 2. Comparison of PSR_{dB} for case-4.

	NMF	APC	DC-APC	G-APC	AMMF
Large non-stationary point target	20.29	30.83	30.13	35.05	35.20
Small stationary point target	0.99	10.93	10.62	10.41	12.13

Fig. 4. Estimated range profile impulse response for each individual range cell using (a) NMF, (b) APC, (c) DC-APC, (d) G-APC, (e) AMMF for case-3.

4.4. Case 4: Large non-stationary point target with closed small stationary target

In this case, two nearby targets are taken to compare the high range resolution capability of NMF, APC, DC-APC, G-APC and the proposed AMMF models. One large moving target along with a small stationary target with $20dB$ less target return power is considered for the simulation purpose.

The range profile with six range cell separated two targets is considered for the simulation purpose. The noise power is set to $-40dB$. The return pulses from the both targets are overlapped and received at the receiver.

In this case, the return from the large moving target is phase shifted by 10° over the full length of the waveform. In Fig. 5, the output of AMMF shows high main lobes resolution with lower side lobes compared to other techniques.

As listed in Table 2, the AMMF model shows the high PSR values for both targets. The AMMF model outperforms the other methods, yet its estimation performance is again degraded due to Doppler mismatch such that the one stationary target is masked by sidelobes.
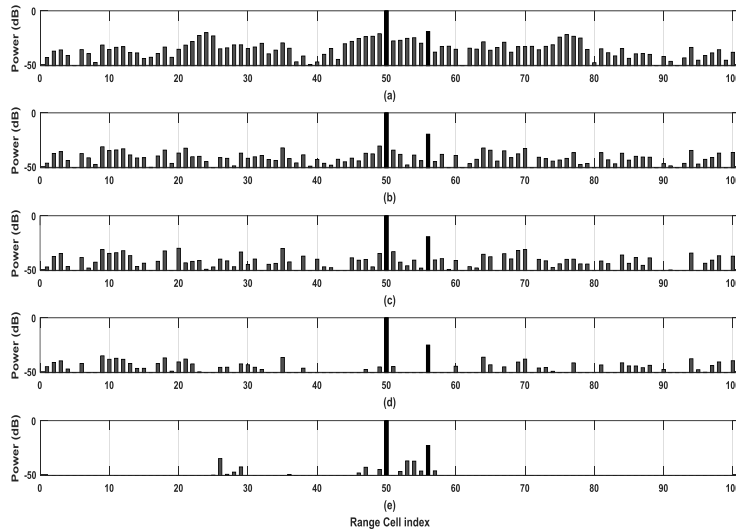
Fig. 5. Estimated range profile impulse response for each individual range cell using (a) NMF, (b) APC, (c) DC-APC, (d) G-APC, (e) AMMF for case-4.

## 4.5. Case 5: Dense target scenario with doppler

In this case, the performance of the proposed AMMF in dense non-stationary targets condition is validated through the simulation study. For the simulation purpose, a large number of stationary and non-stationary point targets of different sizes are considered. The locations, phase shifts due to moving targets and power levels of eight targets are taken randomly. In the range profile, the positions of the targets are $[8, 21, 37, 50, 57, 63, 72, 81]$, the phase shifts over the full length of waveforms are $[13^o, 2^o, -10^o, 18^o, -5^o, 21^o, 10^o, 9^o]$ and the normalized power (dB) are $[-5, -20, -3, 0, -23, -8, -17, -12]$. The noise of -40dB SNR is taken for the simulation purpose. The performance measurements in terms of PSR and outputs of all five methods are shown in Table 3 and Fig. 6, respectively. The ISLR and ATPPA performances are also assessed through a simulation study and are listed in Table 4. These simulation studies show the robustness of AMMF in dense targets scenario. As can be seen in Fig. 6, the AMMF exhibits small sidelobes compared to other pulse compression techniques. The matched filter exhibits the usual range sidelobes masking the smaller targets. The effects of Doppler mismatch are significantly reduced by the AMMF model, resulting in the unmasking of the one small stationary target.

Table 3. Comparison of PSR_{dB} obtained for Case-5.

	NMF	APC	DC-APC	G-APC	AMMF
Target-1	13.66	18.97	21.75	24.01	27.42
Target-2	0.25	3.93	6.71	7.95	8.25
Target-3	15.94	21.18	23.78	26.47	28.58
Target-4	18.56	23.88	27.09	29.01	32.11
Traget-5	Fail	1.55	3.92	3.09	5.36
Target-6	11.74	16.03	19.99	21.02	22.55
Target-7	1.34	6.87	9.84	12.10	12.78
Target-8	6.64	11.92	14.99	16.87	19.27

Table 4. Comparison of $ISLR_{dB}$ and ATPPA (%).

	NMF	APC	DC-APC	G-APC	AMMF
$ISLR_{dB}$	-11.61	-19.65	-21.81	-22.28	-28.33
ATPPA (%)	91.45	98.06	96.37	81.37	95.62
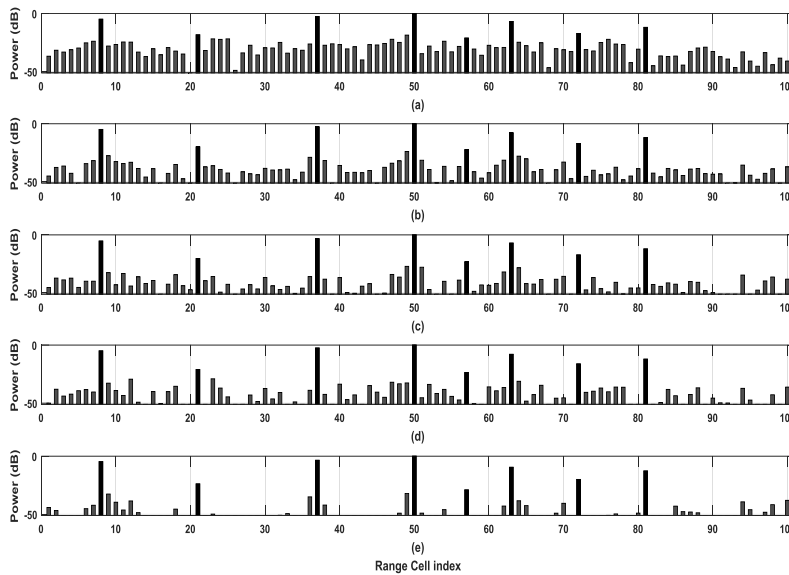
Fig. 6. Estimated range profile impulse response for each individual range cell using (a) NMF, (b) APC, (c) DC-APC, (d) G-APC, (e) AMMF for case-5.

4.6. Complexity evaluation

Since the APC, DC-APC, G-APC and proposed AMMF are the same class of adaptive pulse compression techniques, comparison of the computational cost (Complex Multiplies) is discussed in this section.

It is well known that the computational complexity of all APC, DC-APC and G-APC pulse compression methods depend on the computational load of the first stage. In this stage, NMF is used for estimating the weight coefficients of the next stage. Due to the inversion operation of the matrix, the computational complexity of all these adaptive techniques increases.

In the proposed model, the output of the matched filter has been used for further processing. Unlike the other APC methods, only $N/2$ weight coefficients are required to estimate the range profile impulse response for each range cell.

Comparison of the computational load of all five-pulse compression methods is provided in Table 5. From this table, it may be inferred that for given N and L, the computational load on the AMMF is much less than that of the other adaptive pulse compression methods, however, it is higher than that of NMF

Table 5. Computational Cost (Complex Multiplies).

Methods	Computational cost
NMF	$3N^3 + NL$ (84,000)
APC	$3(2L + 1)N^3 + 5LN + 2L$ (1,62,96,200)
DC-APC	$\dfrac{LN^4}{16} + \left(\dfrac{25L}{4} + 3\right)N^3 + 3LN^2 + \dfrac{11LN}{2} + 2L$ (2,23,05,200)
G-APC	$(8L + 3)N^3 + (3L + 1)N^2 + (5L + 3)N + 2L$ (2,19,67,190)
AMMF	$5LN^3 + (5L + 1)N^3 + \dfrac{11LN}{2}$ (1,39,67,400)

#Value put in brackets is obtained for $N = 30$ and $L = 100$.

5. Conclusions

This paper proposes a novel mismatched filter based on an adaptive pulse compression technique. The received signal is passed through two networks, a linear network with fixed weights, followed by an adaptive linear network. The fixed weight coefficients of the first linear network are similar to the matched filter weight coefficients. The weight coefficients of the adaptive network are estimated using the MMSE based adaptive algorithm. Pulse compression with AMMF model is found to be quite effective in the presence of Doppler shift and in noisy conditions. It is observed that the overall performance of AMMF model is superior to those of the existing adaptive pulse compression methods. Due to non-sequential operations, the computational complexity of the proposed scheme is low, so it can be implemented in most real-time systems.

References

1. Skolnik, M.I. (2015). *Introduction to radar systems* (3rd ed.). Noida, India: McGraw-Hill Education India (Pvt) Ltd.

2. Ackroyd, M.H.; and Ghani, F. (1973). Optimum mismatched filters for sidelobe suppression. *IEEE Transactions on Aerospace and Electronic Systems,* AES-9(2), 214-218.

3. Zoraster, S. (1980). Minimum peak range sidelobe filters for binary phase-coded waveforms. *IEEE Transactions on Aerospace and Electronic Systems,* AES-16(1), 112-115.

4. Baden, J.M.; and Cohen, M.N. (1991). Optimal sidelobe suppression for biphase codes. *Proceedings of National Telesystems Conference (NTC).* Atlanta, Georgia, United States of America, 127-131.

5. Fuentes, E.A.D.R.; and Fam, A.T. (2009). Mismatched filters for Frank polyphase codes via sidelobe inversion. *Proceedings of IEEE Radar Conference*. Pasadena, California, United States of America, 1-6.

6. Levanon, N.; and Scharf, A. (2009). Range sidelobes blanking by comparing outputs of contrasting mismatched filters. *IET Radar, Sonar and Navigation,* 3(3), 265-277.

7. Kumari, U.M.; Rajarajeswari, K.; and Krishna, M.K. (2005). Low sidelobe pattern using Woo filter concepts. *AEU-International Journal of Electronics and Communications*, 59(8), 499-501.

8. Akbaripour, A.; and Bastani, M.H. (2012). Range sidelobe reduction filter design for binary coded pulse compression system. *IEEE Transactions on Aerospace and Electronic Systems*, 48(1), 348-359.

9. Blunt, S.D.; and Gerlach, K. (2006). Adaptive pulse compression via MMSE estimation. *IEEE Transactions on Aerospace and Electronic Systems*, 42(2), 572-584.

10. Blunt, S.D.; Smith, K.J.; and Gerlach, K. (2006). Doppler-compensated adaptive pulse compression. *Proceedings of IEEE Conference on Radar.* Verona, New York, United States of America, 6 pages.

11. Blunt, S.D.; Shackelford, A.K.; Gerlach, K.; and Smith, K.J. (2009). Doppler compensation and single pulse imaging via adaptive pulse compression. *IEEE Transactions on Aerospace and Electronic Systems,* 45(2), 647-659.

12. Blunt, S.D.; and Higgins, T. (2010). Dimensionality reduction techniques for efficient adaptive pulse compression. *IEEE Transactions on Aerospace and Electronic Systems*, 46(1), 349-362.

13. Baghel, V.; and Panda, G. (2013). Development and performance evaluation of generalised Doppler compensated adaptive pulse compression algorithm. *IET Radar, Sonar and Navigation*, 8(4), 297-306.

14. Wang, S.; Li, Z.; Zhang, Y.; Cheong, B.; and Li, L. (2015). Implementation of adaptive pulse compression in solid-state radars: Practical considerations. *IEEE Geoscience and Remote Sensing Letters*, 12(10), 2170-2174.

15. Kikuchi, H.; Yoshikawa, E.; Ushio T.; Mizutani, F.; and Wada, M. (2017). Adaptive pulse compression technique for X-band phased array weather radar. *IEEE Geoscience and Remote Sensing Letters,* 14(10), 1810-1814.

16. Li, Z.; Zhang, Y.; Wang, S.; Li, L.; and Mclinden, M. (2015). Fast adaptive pulse compression based on matched filter outputs. *IEEE Transactions on Aerospace and Electronic Systems*, 51(1), 548-564.

17. Dominguez, E.M.; Magnard, C.; Frioud, M.; Small, D.; and Meier, E. (2017). Adaptive pulse compression for range focusing in SAR imagery. *IEEE Geoscience and Remote Sensing Letters,* 55(04), 2262-2275.

18. Cuprak, T.D.; and Wage, K.E. (2017). Efficient doppler-compensated reiterative minimum mean-squared-error processing. *IEEE Transactions on Aerospace and Electronic Systems*, 53(2), 562-574.

19. Shokooh, R.K.; and Okhovvat, M. (2018). Modified-adaptive pulse compression repair algorithm based on post processing for eclipsing effects. *IET Radar, Sonar and Navigation*, 12(12), 1527-1534.

20. Lewis, B.L.; and Kretschmer, F.F. (1982). Linear frequency modulation derived polyphase pulse compression codes. *IEEE Transactions on Aerospace and Electronic System*, AES-18(5), 637-641.